

# Ground-state magnetic phase diagram of the ferromagnetic Kondo-lattice model

S. Henning\* and W. Nolting

*Lehrstuhl Festkörperteorie, Institut für Physik, Humboldt-Universität zu Berlin, Newtonstrasse 15, 12489 Berlin, Germany*

(Received 21 November 2008; revised manuscript received 14 January 2009; published 12 February 2009)

The magnetic ground-state phase diagram of the ferromagnetic Kondo-lattice model is constructed by explicitly calculating internal energies of all possible bipartite magnetic configurations of the simple cubic lattice. This is done in one, two, and three dimensions for a local moment of  $S=\frac{3}{2}$ . By assuming saturation in the local-moment system we are able to exactly treat all appearing higher local correlation functions within an equation of motion approach. A simple explanation for the obtained phase diagram in terms of bandwidth reduction is given. Regions of phase separation are determined from the internal energy curves by an explicit Maxwell construction.

DOI: 10.1103/PhysRevB.79.064411

PACS number(s): 75.10.Jm, 71.10.Fd, 75.30.Kz, 75.20.Hr

## I. INTRODUCTION

The ferromagnetic Kondo-lattice model (FKLM), also referred to as  $s$ - $d$  model or double exchange model, is the basic model for understanding magnetic phenomena in systems where local magnetic moments couple ferromagnetically to itinerant carriers. This holds for a wide variety of materials.

In the context of transition-metal compounds Zener proposed the double exchange mechanism to explain ferromagnetic (FM) metallic phase in the manganites.<sup>1,2</sup> In these materials the Mn  $5d$  shells are split by the crystal field into three degenerate  $t_{2g}$  orbitals which are localized and form a total spin  $S=\frac{3}{2}$  according to atomic selection rules and two  $e_g$  orbitals providing the itinerant electrons. These electrons couple ferromagnetically via Hund's exchange coupling with the localized spins. Therefore the FKLM is a basic ingredient to describe the rather complex physics of the manganites.<sup>3-5</sup>

Another nearly ideal field of application of the FKLM is the description of the rare-earth materials Gd and EuX ( $X=O, S, Se, Te$ ). These materials have a half-filled  $4f$  shell in common that is strongly localized and the electrons in this shell couple to a total spin momentum of  $S=\frac{7}{2}$ . The FKLM was then used successfully to explain the famous redshift of the absorption edge of the optical  $4f$ - $5d$  transition in the ferromagnetic semiconductor EuO.<sup>6,7</sup> In Ref. 8 a many-body analysis of the FKLM in combination with a band-structure calculation was used to get a realistic value for the Curie temperature of the ferromagnetic metal Gd that is in good agreement with experiment.

Although it is necessary to extend the FKLM in order to get a realistic description of the above-mentioned examples knowledge of the properties of the pure (single band) FKLM is crucial for understanding these materials.

To reveal the ground-state magnetic phases one has to solve the many-body problem of the FKLM. This was already done in previous works by using different techniques. Dynamical mean-field theory (DMFT) was used by several authors<sup>9-12</sup> to get information about different magnetic domains. In Ref. 13 a continuum field theory approach was used to derive the two-dimensional (2D) phase diagram at  $T=0$ . Classical Monte Carlo simulations were performed in Refs. 9 and 14. For 1D systems numerical exact density-matrix renormalization-group calculations were done in Ref.

15. In Ref. 16 the authors have used a Green's-function method to test the validity of assuming the quantum-localized spins to be classical objects. Extended FKLMs including more material specific effects were for instance investigated in Refs. 5 and 17.

In this work we will compare all bipartite magnetic configurations for the simple cubic (sc) lattice by calculating their respective internal energies. To this end the electronic Green's function (GF) has to be determined. This is done by an equation of motion (EQM) approach, and assuming that the local-moment system is saturated, we are able to show that all appearing local higher correlation functions can be treated exactly. From the calculated internal energies the phase diagram is constructed and the region of phase separation is determined.

The paper is organized as follows. In Sec. II the model Hamiltonian and details of the calculation are presented. In Sec. III we discuss the phase diagrams and give an explanation for the sequence of phases obtained by looking at the quasiparticle density of states (QDOS). In Sec. IV we summarize the results and give an outlook on possible directions for further research.

## II. MODEL AND THEORY

### A. Model Hamiltonian

For a proper description of different (anti)ferromagnetic alignments of localized magnetic moments it is useful to divide the full lattice into two or more sublattices (primitive cells) each ordering ferromagnetically.

In this work we only consider simple cubic bipartite lattices, i.e., antiferromagnetic (AFM) configurations that can be obtained by dividing the simple cubic lattice into two sublattices. In Fig. 1 all possible decompositions in two and three dimensions are shown. In case of 1D only the ferromagnetic and  $g$ -type antiferromagnetic phase remain. The Hamiltonian of the FKLM in second quantization reads as follows:

$$H = H_s + H_{SF} = \sum_{ij\sigma} \sum_{\alpha\beta} T_{ij}^{\alpha\beta} c_{i\alpha\sigma}^+ c_{j\beta\sigma} - \frac{J}{2} \sum_{i\sigma} \sum_{\alpha} (z_{\sigma} S_{i\alpha}^z c_{i\alpha\sigma}^+ c_{i\alpha\sigma} + S_{i\alpha}^{\sigma} c_{i\alpha-\sigma}^+ c_{i\alpha\sigma}). \quad (1)$$

The first term describes the hopping of Bloch electrons with

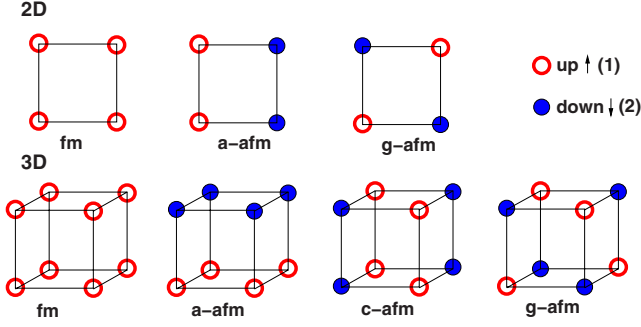


FIG. 1. (Color online) Magnetic phases considered in this work (1D omitted).

spin  $\sigma$  between different sites. The lattice sites  $\mathbf{R}_{i\alpha}$  are denoted by a Latin index  $i$  for the unit cell and a Greek index  $\alpha \in A, B$  for the corresponding sublattice, i.e.,  $\mathbf{R}_{i\alpha} = \mathbf{R}_i + \mathbf{r}_\alpha$ . The second term describes a local Heisenberg-type exchange interaction between the itinerant electrons and local magnetic moments  $\mathbf{S}_{i\alpha}$  where  $J > 0$  is the strength of this interaction,  $z_{\uparrow\downarrow} = \pm 1$  accounts for the two possible spin projections of the electrons, and  $(S_{i\alpha}^\sigma = S_{i\alpha}^x + z_\sigma i S_{i\alpha}^y)$  denotes the spin raising or lowering operator.

### B. Internal energy

The internal energy of the FKLM at  $T=0$  is given by ground-state expectation value of the Hamiltonian:

$$U = \langle H \rangle = \frac{1}{2} \sum_{\alpha\sigma} \int_{-\infty}^{\infty} f_{-}(E) E S_{\alpha\sigma}(E) dE, \quad (2)$$

where  $S_{\alpha\sigma}(E) = -\frac{1}{\pi} \text{Im} G_{\alpha\sigma}(E)$  is the local spectral density,  $f_{-}(E)$  denotes the Fermi function, and  $G_{\alpha\sigma}(E)$  denotes the local electronic GF. Note that this formula is obtained by a straightforward calculation of the ground-state expectation value of Hamiltonian (1) using the spectral theorem and is therefore exact.

Our starting point is the EQM for the electronic GF:

$$\sum_{l\gamma} (E \delta_{il}^{\alpha\gamma} - T_{il}^{\alpha\gamma}) G_{lj\sigma}^{\gamma\beta} = \delta_{ij}^{\alpha\beta} - \frac{J}{2} (I_{ij\sigma}^{\alpha\alpha\beta} + F_{ij\sigma}^{\alpha\alpha\beta}), \quad (3)$$

with Ising-GF,  $I_{ikj\sigma}^{\alpha\gamma\beta} = z_\sigma \langle \langle S_{i\alpha}^z c_{k\gamma\sigma}; c_{j\beta\sigma}^+ \rangle \rangle$ , and spin-flip (SF) GF,  $F_{ikj\sigma}^{\alpha\gamma\beta} = \langle \langle S_{i\alpha}^{-\sigma} c_{k\gamma-\sigma}; c_{j\beta\sigma}^+ \rangle \rangle$ . Our basic assumption for the ground state is perfect saturation of the local-moment system.<sup>18</sup> With this assumption the Ising-GF can be decoupled exactly:

$$I_{ikj\sigma}^{\alpha\gamma\beta}(E) \rightarrow z_\sigma z_\alpha S G_{kj}^{\gamma\beta}(E), \quad (4)$$

where  $z_\alpha = \pm 1$  denotes the direction of sublattice magnetization. In a first attempt to solve Eq. (3) we have neglected spin-flip processes completely ( $F_{ikj\sigma}^{\alpha\gamma\beta} \approx 0$ ). With Eq. (4) we then get a closed system of equations which can be solved for the electronic GF by Fourier transformation:

$$\begin{aligned} G_{\alpha\sigma}^{(\text{MF})}(E) &= \frac{1}{N} \sum_{\mathbf{q}} G_{\mathbf{q}\sigma}^{\alpha\alpha(\text{MF})}(E) \\ &= \frac{1}{N} \sum_{\mathbf{q}} \frac{1}{E + z_\sigma z_\alpha \frac{J}{2} S - \epsilon_{\mathbf{q}}^{\alpha\alpha} - \frac{\epsilon_{\mathbf{q}}^{\alpha\bar{\alpha}} \bar{\epsilon}_{\mathbf{q}}^{\bar{\alpha}\alpha}}{E + z_\sigma z_\alpha \frac{J}{2} S - \epsilon_{\mathbf{q}}^{\bar{\alpha}\bar{\alpha}}}}, \end{aligned} \quad (5)$$

where  $\epsilon_{\mathbf{q}}^{\alpha\beta}$  is the Fourier transform of the hopping integral and  $\bar{\alpha} = -\alpha$  denotes the complementary sublattice. We will call this solution the ‘‘mean-field (MF)’’ solution. Note that the ferromagnetic phase is contained in the above formula by setting  $\epsilon_{\mathbf{q}}^{\alpha\bar{\alpha}}$  to zero.

To go beyond the MF treatment it is necessary to find a better approximation for the spin-flip GF. To this end we write down the EQM for the spin-flip GF:

$$\begin{aligned} \sum_{l\mu} (E \delta_{kl}^{\gamma\mu} - T_{kl}^{\gamma\mu}) F_{ilj\sigma}^{\alpha\mu\beta} &= \langle \langle [S_{i\alpha}^{-\sigma}, H_{\text{SF}}]_{-} c_{k\gamma-\sigma}; c_{j\beta\sigma}^+ \rangle \rangle \\ &+ \langle \langle S_{i\alpha}^{-\sigma} [c_{k\gamma-\sigma}, H_{\text{SF}}]_{-}; c_{j\beta\sigma}^+ \rangle \rangle. \end{aligned} \quad (6)$$

Our strategy to get an approximate solution for the spin-flip GF is to treat the nonlocal correlations on a mean-field level, whereas the local terms will be treated more carefully. This is similar to the idea of the DMFT developed for strongly correlated electron systems.<sup>19</sup> Let us start with the nonlocal ( $i \neq k$  or  $i=k$  but  $\alpha \neq \gamma$ ) GFs first. It can be shown<sup>20</sup> that the higher GFs resulting from the commutator of  $S_{i\alpha}^{-\sigma}$  with  $H_{\text{SF}}$  are approximately given by the product of the spin-flip GF times spin-wave energies of the local-moment system. Therefore it is justified to neglect the resulting GFs since the spin-wave energies are typically 3–4 orders of magnitude smaller than the local coupling  $J$ .<sup>20,21</sup>

The second term on the right-hand side of Eq. (6) gives two higher GFs which we decouple on a mean-field level:

$$\begin{aligned} &\langle \langle S_{i\alpha}^{-\sigma} [c_{k\gamma-\sigma}, H_{\text{SF}}]_{-}; c_{j\beta\sigma}^+ \rangle \rangle \\ &\approx -\frac{J}{2} (\langle \langle S_{i\alpha}^{-\sigma} S_{k\gamma}^{\sigma} \rangle \langle c_{k\gamma\sigma}; c_{j\beta\sigma}^+ \rangle \rangle - z_\sigma \langle S_{k\gamma}^z \rangle \langle \langle S_{i\alpha}^{-\sigma} c_{k\gamma-\sigma}; c_{j\beta\sigma}^+ \rangle \rangle) \\ &\rightarrow z_\sigma z_\gamma S \frac{J}{2} F_{ikj\sigma}^{\alpha\gamma\beta}, \end{aligned} \quad (7)$$

where in the last step the saturated sublattice magnetization is exploited.

We now come to the local terms ( $i=k$  and  $\alpha=\gamma$ ). The two higher GFs resulting from the second commutator on the right-hand side of Eq. (6) reduce to

$$\begin{aligned} &\langle \langle S_{i\alpha}^{-\sigma} S_{i\alpha}^{\sigma} c_{i\alpha\sigma}; c_{j\beta\sigma}^+ \rangle \rangle \rightarrow S(1 - z_\sigma z_\alpha) G_{ij\sigma}^{\alpha\beta}, \\ &\langle \langle S_{i\alpha}^{-\sigma} S_{i\alpha}^z c_{i\alpha-\sigma}; c_{j\beta\sigma}^+ \rangle \rangle \rightarrow (z_\alpha S + z_\sigma \delta_{-\sigma\alpha}) F_{ij\sigma}^{\alpha\alpha\beta}. \end{aligned} \quad (8)$$

Additionally we get a higher-order Ising-GF and spin-flip GF from the first commutator. The higher-order spin-flip GF can be treated *exactly* by using the EQM of the (known) Ising-GF given in Eq. (A1). This leads to

$$\begin{aligned}
& \langle\langle S_{i\alpha}^{-\sigma} n_{i\alpha\sigma} c_{i\alpha-\sigma}^+; c_{j\beta\sigma}^+ \rangle\rangle \\
& \rightarrow z_{\sigma} z_{\alpha} \frac{2}{J} S \left\{ \delta_{ij}^{\alpha\beta} - \sum_{l\mu} \left[ \left( E + z_{\sigma} z_{\alpha} \frac{J}{2} S \right) \delta_{il}^{\alpha\mu} - T_{il}^{\alpha\mu} \right] G_{lj\sigma}^{\mu\beta} \right\} \\
& - (z_{\sigma} z_{\alpha} S - \delta_{\sigma\alpha}) F_{ij\sigma}^{\alpha\beta}. \quad (9)
\end{aligned}$$

The higher-order Ising-GF can be traced back to the higher-order spin-flip GF by writing down its EQM and making use of saturation in the local-moment system (see Appendix B for details):

$$\begin{aligned}
& \langle\langle S_{i\alpha}^z n_{i\alpha-\sigma} c_{i\alpha\sigma}^+; c_{j\beta\sigma}^+ \rangle\rangle \rightarrow z_{\alpha} S \left( G_{ij\sigma}^{\alpha\beta(\text{MF})} \langle n_{j\beta-\sigma} \rangle - \frac{J}{2} \sum_{l\gamma} G_{il\sigma}^{\alpha\gamma(\text{MF})} \right. \\
& \left. \times \langle\langle S_{l\gamma}^{-\sigma} n_{l\gamma\sigma} c_{l\gamma-\sigma}^+; c_{j\beta\sigma}^+ \rangle\rangle \right). \quad (10)
\end{aligned}$$

It is a major result of this work that it is possible to incorporate all local correlations without approximation, i.e., to treat all local higher-order GFs exactly. Combining the results for the appearing higher GFs found in Eqs. (7), (9), and (10), we can now solve Eq. (6) for the spin-flip GF:

$$\begin{aligned}
F_{ij\sigma}^{\alpha\beta} = & - \frac{J S G_{\alpha-\sigma}^{\text{MF}}}{1 + z_{\sigma} z_{\alpha} \frac{J}{2} G_{\alpha-\sigma}^{\text{MF}}} \left\{ z_{\sigma} z_{\alpha} G_{ij\sigma}^{\alpha\beta(\text{MF})} (\langle n_{j-\sigma}^{\beta} \rangle - \delta_{\sigma\beta}) \right. \\
& \left. + \sum_{l\gamma} \left[ \delta_{il}^{\alpha\gamma} \delta_{\sigma-\alpha} + G_{il\sigma}^{\alpha\gamma(\text{MF})} \delta_{\sigma\gamma} \sum_{l\eta} (G_{jk\sigma}^{\mu\nu(\text{MF})})_{ll}^{-1\gamma\eta} \right] G_{lj\sigma}^{\eta\beta} \right\}. \quad (11)
\end{aligned}$$

Inserting this result into Eq. (3) and performing a Fourier transformation we finally get

$$\begin{aligned}
& \sum_{\gamma} \left( [G_{q\sigma}^{\mu\nu(\text{MF})}]_{A\gamma}^{-1} - A_{\sigma l}^{\alpha l} \delta_{\sigma-\alpha} \delta_{\alpha\gamma} + G_{q\sigma}^{\alpha\sigma(\text{MF})} [G_{q\sigma}^{\mu\nu(\text{MF})}]_{J\gamma\beta}^{-1} \right) G_{q\sigma}^{\gamma\beta}(E) \\
& = \delta_{\alpha\beta} + z_{\sigma} z_{\alpha} A_{\sigma}^{\alpha} G_{q\sigma}^{\alpha\beta(\text{MF})} (\langle n_{-\sigma}^{\beta} \rangle - \delta_{\sigma\beta}), \quad (12)
\end{aligned}$$

with

$$A_{\sigma}^{\alpha}(E) = \frac{J^2 S G_{\alpha-\sigma}^{\text{MF}}(E)}{2 + z_{\sigma} z_{\alpha} J G_{\alpha-\sigma}^{\text{MF}}(E)}.$$

This equation allows for a self-consistent calculation of the electronic GF, and we will call this the SF solution.

One important test for the above result is to compare it with exact known limiting cases. We found that Eq. (12) reproduces the solution of the ferromagnetically saturated semiconductor<sup>22,23</sup> in the limit of zero band occupation. Additionally the four-peak structure of the spectrum as known from the “zero-bandwidth” limit<sup>24</sup> is retained, whereas the peaks are broadened to bands with their center of gravity at the original peak positions.

### C. Phase separation

To determine the regions of phase separation in the phase diagram we have used an explicit Maxwell construction as shown in Fig. 2. The condition for the boundaries of the phase separated region is

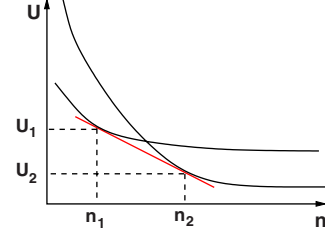


FIG. 2. (Color online) Explicit Maxwell construction for determining the boundaries of phase separated regions.

$$\left. \frac{dU_1}{dn} \right|_{n=n_1} = \frac{U_2(n_2) - U_1(n_1)}{n_2 - n_1} = \left. \frac{dU_2}{dn} \right|_{n=n_2}. \quad (13)$$

## III. RESULTS AND DISCUSSION

The internal energy of the FKLm at  $T=0$  is given as an integral [Eq. (2)] over the product of (sublattice) QDOS times energy up to Fermi energy. For understanding the resulting phase diagrams it is therefore useful to have a closer look at the QDOS first. In Fig. 3 the sublattice MF-QDOS is shown for the different magnetic phases investigated (in three dimensions). The underlying full lattice is of simple cubic type with nearest-neighbor hopping  $T$  chosen such that the bandwidth  $W$  is equal to  $W=1$  eV in the case of free electrons ( $J=0$  eV). The local magnetic moment is equal to  $S=\frac{3}{2}$ . We have plotted the up-electron and down-electron spectra separately for two different values of  $J=0.1/1.0$  eV. The exchange splitting  $\Delta_{\text{ex}}=JS$  eV of up and down bands is clearly visible. The decisive difference between the phases for nonzero values of  $J$  is bandwidth reduction from ferromagnetic over  $A, C$  to  $G$ -AFM phase. The reason for this behavior becomes clear by looking at the magnetic lattices shown in Fig. 1. In the ferromagnetic case an (up) electron can move freely in all three directions of space without paying any additional potential energy. In  $A$ -type antiferromagnetic phase the electron can still move freely within a plane, but when moving in the direction perpendicular to the plane it needs to overcome an energy barrier  $\Delta_{\text{ex}}$ . Hence the QDOS for large values of  $J$  resembles the form of 2D tight-binding

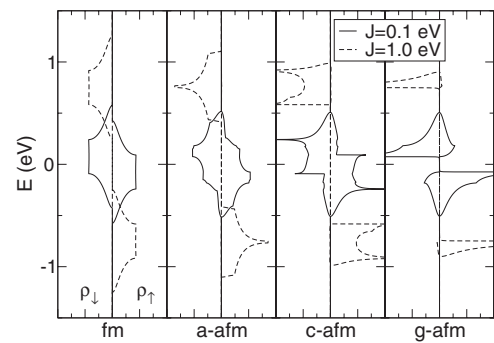


FIG. 3. Sublattice QDOS of up and down electrons obtained from the MF-GF [Eq. (5)] for two values of local coupling  $J$  shown for different magnetic configurations. Parameters:  $S=\frac{3}{2}$  and free-electron bandwidth:  $W=1.0$  eV.

dispersion. The bandwidth is reduced due to the confinement of the electrons. In the *C*-AFM phase the electron can only move freely along one direction, and the QDOS becomes effectively one dimensional (1D). Finally in the *G*-type phase the electron in the large  $J$  limit is quasilocalized and the bandwidth gets very small. We will see soon that this bandwidth effect is mainly responsible for the structure of the phase diagram. Before we come to this point we want to discuss the influence of spin-flip processes as incorporated in Eq. (12). In Fig. 4 the QDOS for  $J=0.5$  eV is shown for three different band fillings  $n$ . The corresponding Fermi energies are marked by horizontal lines. The apparent new feature is the scattering states in the down spectrum for band fillings below half filling. Thereby the spectral weight of the scattering states is more and more reduced with increasing Fermi level. A second effect is that the sharp features in the MF-QDOS of the antiferromagnetic phases are smeared out. Compared to the MF results the overall change in QDOS below Fermi energy due to the inclusion of spin-flip processes is small and will not drastically affect the form of the phase diagram. However non-negligible changes can be expected. Note that the model shows perfect particle-hole symmetry. Therefore the results for the internal energy will be

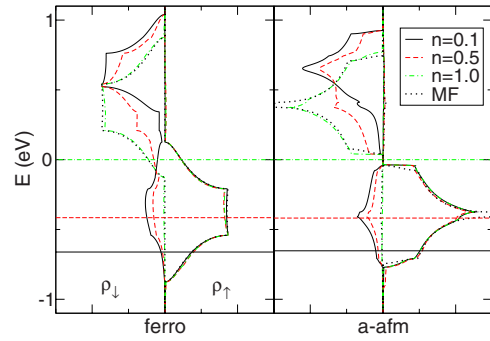


FIG. 4. (Color online) Sublattice QDOS of up and down electrons obtained from the SF-GF [Eq. (12)] for three different band fillings  $n$  shown for the ferromagnetic and *a*-AFM phase. The local coupling  $J=0.5$  eV is fixed. Dotted line: corresponds to MF result. Horizontal lines: respective Fermi levels. Other parameters as shown in Fig. 3.

the same for  $n=x$  and  $n=2-x$  ( $x=0\dots 1$  and  $n=1$ : half filling).

We come now to the discussion of the phase diagrams which we got by explicitly comparing the internal energies of the different phases. The pure phase diagrams (without

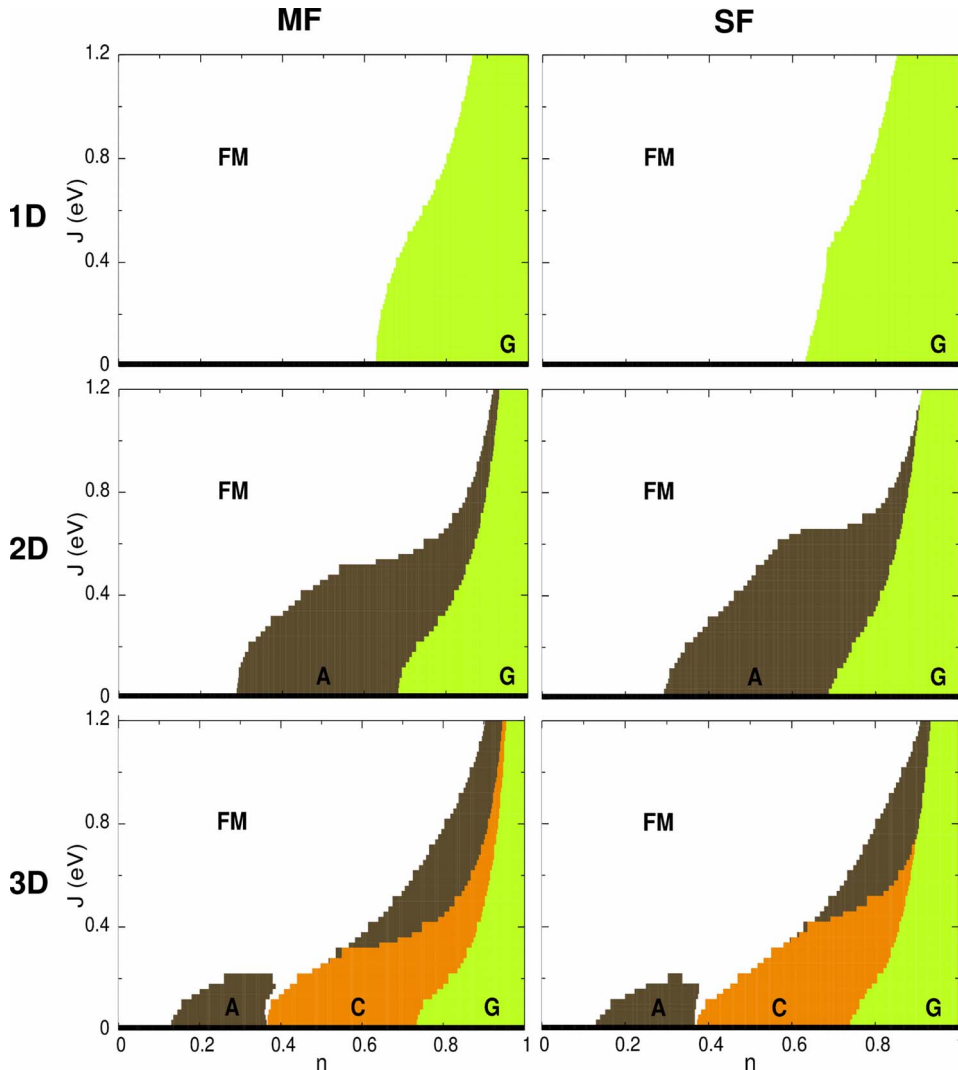


FIG. 5. (Color online) First column: phase diagram as function of band filling  $n$  and local coupling  $J$  obtained with MF theory (6) in one, two, and three dimensions. Second column: phase diagram obtained by inclusion of SF processes [Eq. (12)]. Regions of different colors mark different (magnetic) phases: ferromagnetic (white), *A*-AFM (brown), *C*-AFM (orange), *G*-AFM (green), and paramagnetic phase (black).

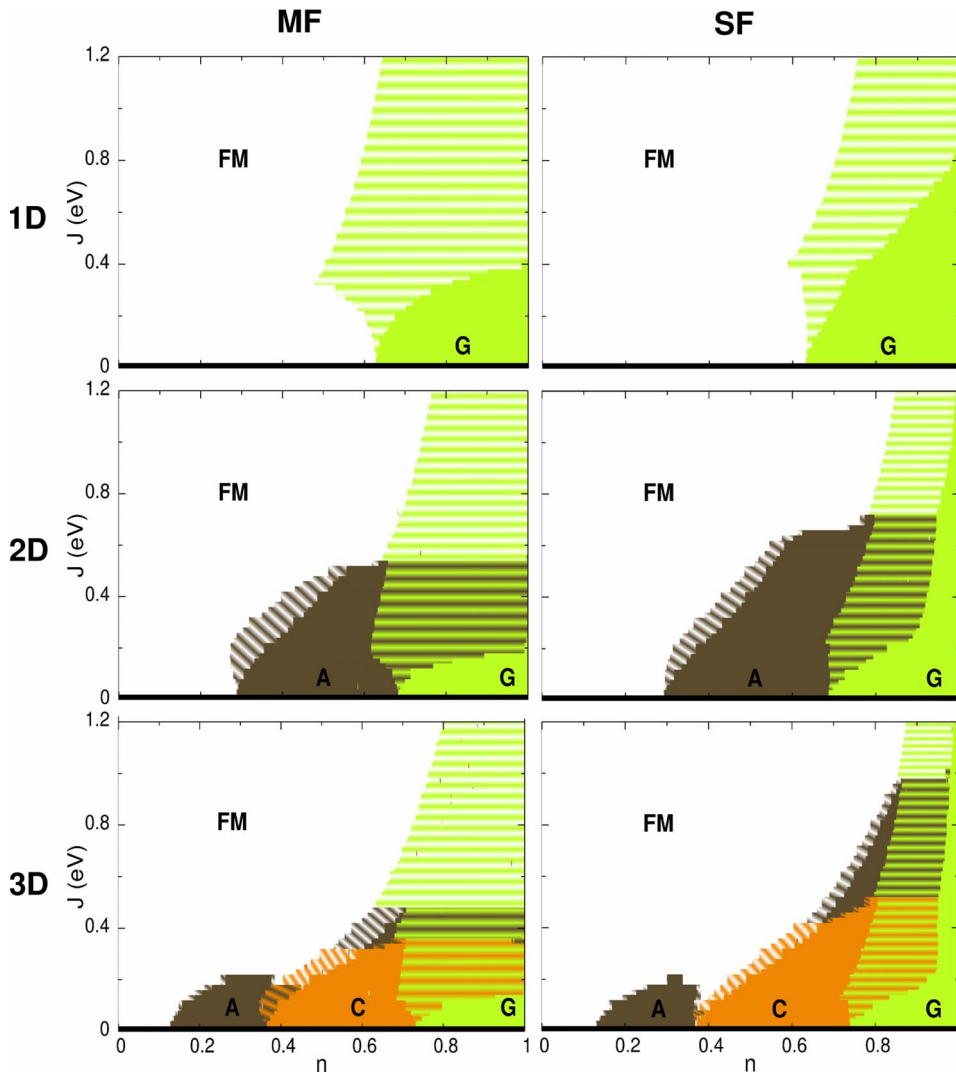


FIG. 6. (Color online) Phase diagram with phase separation. Regions of phase separation are marked with two-colored stripes. Color codes the same as in Fig. 5.

phase separation) are shown in Fig. 5, whereas the different phases are marked by color code. In the first column the results of the MF calculation are shown for the 1D, 2D, and 3D cases. The second column shows the effects of inclusion of spin-flip processes. We will concentrate here mainly onto the 3D case since most of the given arguments hold equally for the 1D and 2D cases. For  $J=0$  the system is paramagnetic (black bar at bottom). For larger  $J$  ( $J>0$ ) a typical sequence appears: for low band fillings  $n$  the system is always ferromagnetic, and with increasing  $n$ , it becomes  $A$ -type, then  $C$ -type, and finally  $G$ -type antiferromagnetic. This behavior is understood easily by looking at the formula for the internal energy [Eq. (2)] and the MF-QDOS in Fig. 3. Because of the bandwidth effect discussed already the band edge of the ferromagnetic state is always lowest in energy and will give therefore the lowest internal energy for small band occupation. But since the QDOS of the antiferromagnetic phases increase much more rapidly than the ferromagnetic one, these give more weight to low energies in integral (2) and will become lowest in energy eventually for larger band fillings. Therefore the bandwidth effect is the main effect explaining the order of phases with increasing  $n$ . A very interesting feature can be found in the region:  $J=0.2\dots 0.3$ . In this

region the ferromagnetic phase is directly followed by the  $C$ -AFM phase for increasing  $n$  although the  $A$ -AFM phase has a larger bandwidth than the  $C$ -AFM phase. This can be explained by the two-peak structure of the  $C$ -AFM QDOS. Due to the first peak at low energies these energies are much more weighted than in the  $A$ -AFM case and the  $C$ -AFM phase will become lower in energy than the  $A$ -AFM phase. Since the reduction in bandwidth of the antiferromagnetic phases compared to the ferromagnetic phase is more pronounced for larger values of  $J$ , the ferromagnetic region is growing in this direction.

The paramagnetic phase (black bar at  $J=0$ ) disappears for any finite  $J$  since due to the downshift of the up spectrum of the ferromagnetic phase their internal energy will always be lower. When comparing the MF and the SF phase diagrams they appear to be very similar at first glance. However two interesting differences can be found, namely, an increased  $J$  region without  $A$ -AFM phase and the vanishing  $C$  phase above  $J\approx 0.8$  eV.

Figure 6 shows the phase diagrams where regions of phase separation, which we have determined by an explicit Maxwell construction [Eq. (13)], are marked by colored stripes. The two colors denote the involved pure phases. As

one can see large regions become phase separated, whereas the two participating phases are mostly determined by the adjacent pure phases. There is one interesting exception from this: above a certain  $J$  only FM/ $G$ -AFM phase separation survives and suppresses all other phases in this area. Inclusion of spin-flip processes as shown in the right column of Fig. 6 push this  $J$  up to higher values. Generally spin-flip processes seem to reduce phase separation as can be seen in the  $G$ -AFM phase and, e.g., at the border between FM and  $C$ -AFM phases.

Our results are in good qualitative agreement with numerical and DMFT results reported by others.<sup>11,12,14</sup> It is common to all these works that for small coupling strength  $J$  there is only a small ferromagnetic region at low band occupation  $n$  followed by more complicated (antiferromagnetic, spiral, and canted) spin states or phase separation. With increasing  $J$  the region of FM is also increased to larger  $n$  values. Near half filling ( $n=1$ ) one will always find antiferromagnetism or phase separation. The phase-diagram very similar to our 2D-FM result shown in Fig. 6 was obtained by Pekker *et al.*<sup>13</sup> The positions of  $A$  and  $G$  phases are in nearly perfect agreement. However the authors seem not to have taken into account phase separation between  $A$  and  $G$  phases and their finding of FM/ $A$  phase separation near half filling at larger  $J$  is not in accordance with our results.

#### IV. SUMMARY AND OUTLOOK

We have constructed phase diagrams of the FKLM in 1D, 2D, and 3D by comparing the internal energies of all possible bipartite magnetic configurations of the simple cubic lattice. To this end the electronic GF is calculated by an EQM approach. We can show that it is possible to treat all appearing higher local correlation functions exactly and derive an explicit formula for the electronic GF [Eq. (12)]. The obtained sequence of phases with increasing band occupation  $n$  and Hund's coupling  $J$  is explained by the reduction in QDOS bandwidth due to electron confinement. Region of phase separation are then determined from the internal energy curves by an explicit Maxwell construction.

In the phase diagram obtained only phases appear that have explicitly considered by us. Therefore an important extension of this work could be the inclusion of more complicated spin structures such as canted or spiral spin states as reported by others.<sup>13,15</sup> However the bandwidth criterion obtained here can certainly be applied to such more complicated states also.

#### APPENDIX A: EQM OF THE ISING-GF

$$\begin{aligned} \sum_{l\mu} (E \delta_{kl}^{\gamma\mu} - T_{kl}^{\gamma\mu}) I_{ilj\sigma}^{\alpha\mu\beta} &= z_{\sigma} \delta_{kj}^{\gamma\beta} \langle S_{i\alpha}^z \rangle - \frac{J}{2} (\langle \langle S_{i\alpha}^z S_{k\gamma}^z c_{k\gamma\sigma}; c_{j\beta\sigma}^+ \rangle \rangle \\ &+ z_{\sigma} \langle \langle S_{i\alpha}^z S_{k\gamma}^{-\sigma} c_{k\gamma\sigma}; c_{j\beta\sigma}^+ \rangle \rangle \\ &+ z_{\sigma} \sum_{\sigma'} z_{\sigma'} \langle \langle S_{i\alpha}^{\sigma'} c_{i\alpha-\sigma'}^+ c_{i\alpha\sigma'} c_{k\gamma\sigma}; c_{j\beta\sigma}^+ \rangle \rangle). \end{aligned} \quad (\text{A1})$$

#### APPENDIX B: HIGHER-ORDER ISING-GF

The higher-order Ising-GF can be decomposed into

$$\langle \langle S_{i\alpha}^z n_{i\alpha-\sigma} c_{i\alpha\sigma}; c_{j\beta\sigma}^+ \rangle \rangle \rightarrow z_{\alpha} S \langle \langle n_{i\alpha-\sigma} c_{i\alpha\sigma}; c_{j\beta\sigma}^+ \rangle \rangle \quad (\text{B1})$$

when a saturated sublattice magnetization is assumed. The EQM of the remaining GF turns out to be

$$\begin{aligned} &\left( E + z_{\sigma} z_{\alpha} \frac{J}{2} S \right) \langle \langle n_{i\alpha-\sigma} c_{i\alpha\sigma}; c_{j\beta\sigma}^+ \rangle \rangle \\ &= \sum_{l\gamma} T_{il}^{\alpha\gamma} \langle \langle c_{l\gamma-\sigma}^+ c_{i\alpha-\sigma} c_{i\alpha\sigma}; c_{j\beta\sigma}^+ \rangle \rangle \quad (\text{I}) \\ &+ \sum_{l\gamma} T_{il}^{\alpha\gamma} \langle \langle c_{i\alpha-\sigma}^+ c_{l\gamma-\sigma} c_{i\alpha\sigma}; c_{j\beta\sigma}^+ \rangle \rangle \quad (\text{II}) \\ &+ \sum_{l\gamma} T_{il}^{\alpha\gamma} \langle \langle c_{i\alpha-\sigma}^+ c_{i\alpha-\sigma} c_{l\gamma\sigma}; c_{j\beta\sigma}^+ \rangle \rangle \quad (\text{III}) \\ &- 2 \sum_{l\gamma} T_{il}^{\alpha\gamma} \langle \langle c_{l\gamma-\sigma}^+ c_{i\alpha-\sigma} c_{i\alpha\sigma}; c_{j\beta\sigma}^+ \rangle \rangle + \delta_{ij}^{\alpha\beta} \langle n_{i\alpha-\sigma} \rangle \\ &- \frac{J}{2} \langle \langle S_{i\alpha}^{-\sigma} n_{i\alpha\sigma} c_{i\alpha-\sigma}; c_{j\beta\sigma}^+ \rangle \rangle. \end{aligned} \quad (\text{B2})$$

Subtracting the term denoted by (I) from this equation one gets

$$\begin{aligned} &\sum_{l\gamma} \left( E \delta_{il}^{\alpha\gamma} - T_{il}^{\alpha\gamma} + z_{\sigma} z_{\alpha} \delta_{il}^{\alpha\gamma} \frac{J}{2} S \right) \langle \langle c_{l\gamma-\sigma}^+ c_{i\alpha-\sigma} c_{i\alpha\sigma}; c_{j\beta\sigma}^+ \rangle \rangle \\ &= \sum_{l\gamma} T_{il}^{\alpha\gamma} \langle \langle c_{i\alpha-\sigma}^+ c_{l\gamma-\sigma} c_{i\alpha\sigma}; c_{j\beta\sigma}^+ \rangle \rangle \\ &+ \sum_{l\gamma} T_{il}^{\alpha\gamma} \langle \langle c_{i\alpha-\sigma}^+ c_{i\alpha-\sigma} c_{l\gamma\sigma}; c_{j\beta\sigma}^+ \rangle \rangle \\ &- 2 \sum_{l\gamma} T_{il}^{\alpha\gamma} \langle \langle c_{l\gamma-\sigma}^+ c_{i\alpha-\sigma} c_{i\alpha\sigma}; c_{j\beta\sigma}^+ \rangle \rangle + \delta_{ij}^{\alpha\beta} \langle n_{i\alpha-\sigma} \rangle \\ &- \frac{J}{2} \langle \langle S_{i\alpha}^{-\sigma} n_{i\alpha\sigma} c_{i\alpha-\sigma}; c_{j\beta\sigma}^+ \rangle \rangle. \end{aligned} \quad (\text{B3})$$

This can be solved for  $\langle \langle n_{i\alpha-\sigma} c_{i\alpha\sigma}; c_{j\beta\sigma}^+ \rangle \rangle$  by left-multiplying with the MF-GF matrix,

$$\begin{aligned} \langle \langle n_{i\alpha-\sigma} c_{i\alpha\sigma}; c_{i\alpha\sigma}^+ \rangle \rangle &= \sum_{kl\eta\gamma} G_{ik\sigma}^{(\text{MF})\alpha\eta} T_{kl}^{\eta\gamma} \langle \langle c_{i\alpha-\sigma}^+ c_{l\gamma-\sigma} c_{i\alpha\sigma}; c_{j\beta\sigma}^+ \rangle \rangle \\ &+ \sum_{kl\eta\gamma} G_{ik\sigma}^{(\text{MF})\alpha\eta} T_{kl}^{\eta\gamma} \langle \langle c_{i\alpha-\sigma}^+ c_{i\alpha-\sigma} c_{l\gamma\sigma}; c_{j\beta\sigma}^+ \rangle \rangle \\ &- 2 \sum_{kl\eta\gamma} G_{ik\sigma}^{(\text{MF})\alpha\eta} T_{kl}^{\eta\gamma} \langle \langle c_{l\gamma-\sigma}^+ c_{i\alpha-\sigma} c_{i\alpha\sigma}; c_{j\beta\sigma}^+ \rangle \rangle \\ &+ G_{ij\sigma}^{(\text{MF})\alpha\beta} \langle n_{j\beta-\sigma} \rangle \\ &- \frac{J}{2} \sum_{k\eta} G_{ik\sigma}^{(\text{MF})\alpha\eta} \langle \langle S_{k\eta}^{-\sigma} n_{k\eta\sigma} c_{k\eta-\sigma}; c_{j\beta\sigma}^+ \rangle \rangle. \end{aligned} \quad (\text{B4})$$

Two other equations are obtained from Eq. (B2) by subtracting term (II) or (III) and performing the same steps as before. These yields

$$\begin{aligned}
\langle\langle n_{i\alpha-\sigma}c_{i\alpha\sigma}; c_{i\alpha\sigma}^+ \rangle\rangle &= \sum_{kl\eta\gamma} G_{ik\sigma}^{(\text{MF})\alpha\eta} T_{kl}^{\eta\gamma} \langle\langle c_{l\gamma-\sigma}^+ c_{i\alpha-\sigma} c_{i\alpha\sigma}; c_{j\beta\sigma}^+ \rangle\rangle \\
&+ \sum_{kl\eta\gamma} G_{ik\sigma}^{(\text{MF})\alpha\eta} T_{kl}^{\eta\gamma} \langle\langle c_{i\alpha-\sigma}^+ c_{i\alpha-\sigma} c_{l\gamma\sigma}; c_{j\beta\sigma}^+ \rangle\rangle \\
&- 2 \sum_{kl\eta\gamma} G_{ik\sigma}^{(\text{MF})\alpha\eta} T_{kl}^{\eta\gamma} \langle\langle c_{l\gamma-\sigma}^+ c_{i\alpha-\sigma} c_{i\alpha\sigma}; c_{j\beta\sigma}^+ \rangle\rangle \\
&+ G_{ij\sigma}^{(\text{MF})\alpha\beta} \langle n_{j\beta-\sigma} \rangle \\
&- \frac{J}{2} \sum_{k\eta} G_{ik\sigma}^{(\text{MF})\alpha\eta} \langle\langle S_{k\eta}^{-\sigma} n_{k\eta\sigma} c_{k\eta-\sigma}; c_{j\beta\sigma}^+ \rangle\rangle
\end{aligned} \tag{B5}$$

and

$$\begin{aligned}
\langle\langle n_{i\alpha-\sigma}c_{i\alpha\sigma}; c_{i\alpha\sigma}^+ \rangle\rangle &= \sum_{kl\eta\gamma} G_{ik\sigma}^{(\text{MF})\alpha\eta} T_{kl}^{\eta\gamma} \langle\langle c_{l\gamma-\sigma}^+ c_{i\alpha-\sigma} c_{i\alpha\sigma}; c_{j\beta\sigma}^+ \rangle\rangle \\
&+ \sum_{kl\eta\gamma} G_{ik\sigma}^{(\text{MF})\alpha\eta} T_{kl}^{\eta\gamma} \langle\langle c_{i\alpha-\sigma}^+ c_{l\gamma-\sigma} c_{i\alpha\sigma}; c_{j\beta\sigma}^+ \rangle\rangle \\
&- 2 \sum_{kl\eta\gamma} G_{ik\sigma}^{(\text{MF})\alpha\eta} T_{kl}^{\eta\gamma} \langle\langle c_{l\gamma-\sigma}^+ c_{i\alpha-\sigma} c_{i\alpha\sigma}; c_{j\beta\sigma}^+ \rangle\rangle
\end{aligned}$$

$$\begin{aligned}
&+ G_{ij\sigma}^{(\text{MF})\alpha\beta} \langle n_{j\beta-\sigma} \rangle \\
&- \frac{J}{2} \sum_{k\eta} G_{ik\sigma}^{(\text{MF})\alpha\eta} \langle\langle S_{k\eta}^{-\sigma} n_{k\eta\sigma} c_{k\eta-\sigma}; c_{j\beta\sigma}^+ \rangle\rangle.
\end{aligned} \tag{B6}$$

Adding Eqs. (B5) and (B6) and subtracting Eq. (B4) one finally gets

$$\begin{aligned}
\langle\langle S_{i\alpha}^z n_{i\alpha-\sigma} c_{i\alpha\sigma}; c_{j\beta\sigma}^+ \rangle\rangle &= z_\alpha S \left( G_{ij\sigma}^{\alpha\beta(\text{MF})} \langle n_{j\beta-\sigma} \rangle - \frac{J}{2} \sum_{l\gamma} G_{il\sigma}^{\alpha\gamma(\text{MF})} \right. \\
&\times \left. \langle\langle S_{l\gamma}^{-\sigma} n_{l\gamma\sigma} c_{l\gamma-\sigma}; c_{j\beta\sigma}^+ \rangle\rangle \right).
\end{aligned} \tag{B7}$$

\*henning@physik.hu-berlin.de

<sup>1</sup>C. Zener, Phys. Rev. **81**, 440 (1951).

<sup>2</sup>C. Zener, Phys. Rev. **82**, 403 (1951).

<sup>3</sup>E. Dagotto, *Nanoscale Phase Separation and Colossal Magnetoresistance* (Springer, Berlin, 2003).

<sup>4</sup>M. Stier and W. Nolting, Phys. Rev. B **75**, 144409 (2007).

<sup>5</sup>M. Stier and W. Nolting, Phys. Rev. B **78**, 144425 (2008).

<sup>6</sup>G. Busch, P. Junod, and P. Wachter, Phys. Lett. **12**, 11 (1964).

<sup>7</sup>F. Rys, J. S. Helman, and W. Baltensperger, Phys. Kondens. Mater. **6**, 105 (1967).

<sup>8</sup>C. Santos, W. Nolting, and V. Eyert, Phys. Rev. B **69**, 214412 (2004).

<sup>9</sup>S. Yunoki, J. Hu, A. L. Malvezzi, A. Moreo, N. Furukawa, and E. Dagotto, Phys. Rev. Lett. **80**, 845 (1998).

<sup>10</sup>M. Y. Kagan, D. I. Khomskii, and M. V. Mostovoy, Eur. Phys. J. B **12**, 217 (1999).

<sup>11</sup>A. Chattopadhyay, A. J. Millis, and S. Das Sarma, Phys. Rev. B **64**, 012416 (2001).

<sup>12</sup>C. Lin and A. J. Millis, Phys. Rev. B **72**, 245112 (2005).

<sup>13</sup>D. Pekker, S. Mukhopadhyay, N. Trivedi, and P. M. Goldbart, Phys. Rev. B **72**, 075118 (2005).

<sup>14</sup>E. Dagotto, S. Yunoki, A. L. Malvezzi, A. Moreo, J. Hu, S. Capponi, D. Poilblanc, and N. Furukawa, Phys. Rev. B **58**, 6414 (1998).

<sup>15</sup>D. J. Garcia, K. Hallberg, B. Alascio, and M. Avignon, Phys. Rev. Lett. **93**, 177204 (2004).

<sup>16</sup>J. Kienert and W. Nolting, Phys. Rev. B **73**, 224405 (2006).

<sup>17</sup>R. Peters and T. Pruschke, Phys. Rev. B **76**, 245101 (2007).

<sup>18</sup>Although it is known that the Neel state is not the ground state of a Heisenberg antiferromagnet deviations from saturation are small for a local magnetic moment  $S > \frac{1}{2}$  (see, e.g., Ref. 25).

<sup>19</sup>A. Georges, G. Kotliar, W. Krauth, and M. J. Rozenberg, Rev. Mod. Phys. **68**, 13 (1996).

<sup>20</sup>W. Nolting, S. Rex, and S. Mathi Jaya, J. Phys.: Condens. Matter **9**, 1301 (1997).

<sup>21</sup>C. Santos and W. Nolting, Phys. Rev. B **65**, 144419 (2002).

<sup>22</sup>B. S. Shastry and D. C. Mattis, Phys. Rev. B **24**, 5340 (1981).

<sup>23</sup>S. R. Allan and D. M. Edwards, J. Phys. C **15**, 2151 (1982).

<sup>24</sup>W. Nolting and M. Matlak, Phys. Status Solidi B **123**, 155 (1984).

<sup>25</sup>P. W. Anderson, Phys. Rev. **86**, 694 (1952).